


Exosomes Derived from Antler Mesenchymal Stem Cells Promote Wound Healing by miR-21-5p/STAT3 Axis

Deshuang Meng, Yingrui Li, Ze Chen, Jia Guo, Min Yang, Yinghua Peng 

Institute of Special Animal and Plant Sciences, Chinese Academy of Agricultural Sciences, Changchun, Jilin, 130112, People's Republic of China

Correspondence: Yinghua Peng; Min Yang, Institute of Special Animal and Plant Sciences, Chinese Academy of Agricultural Sciences, Changchun, Jilin, 130112, People's Republic of China, Email pengyinghua@caas.cn; yangmin01@caas.cn

Background: Deer antlers, unique among mammalian organs for their ability to regenerate annually without scar formation, provide an innovative model for regenerative medicine. This study explored the potential of exosomes derived from antler mesenchymal stem cells (AMSC-Exo) to enhance skin wound healing.

Methods: We explored the proliferation, migration and angiogenesis effects of AMSC-Exo on HaCaT cells and HUVEC cells. To investigate the skin repairing effect of AMSC-Exo, we established a full-thickness skin injury mouse model. Then the skin thickness, the epidermis, collagen fibers, CD31 and collagen expressions were tested by H&E staining, Masson's trichrome staining and immunofluorescence experiments. MiRNA omics analysis was conducted to explore the mechanism of AMSC-Exo in skin repairing.

Results: AMSC-Exo stimulated the proliferation and migration of HaCaT cells, accelerated the migration and angiogenesis of HUVEC cells. In the mouse skin injury model, AMSC-Exo stimulated angiogenesis and regulated the extracellular matrix by facilitating the conversion of collagen type III to collagen type I, restoring epidermal thickness to normal state without aberrant hyperplasia. Notably, AMSC-Exo enhanced the quality of wound healing with increased vascularization and reduced scar formation. MiRNAs in AMSC-Exo, especially through the miR-21-5p/STAT3 signaling pathway, played a crucial role in these processes.

Conclusion: This study underscores the efficacy of AMSC-Exo in treating skin wounds, suggesting a new approach for enhancing skin repair and regeneration.

Keywords: deer antler, mesenchymal stem cells, exosomes, microRNA, skin wound healing

Introduction

Skin, the largest organ of the human body, performs crucial physiological functions such as regulating body temperature, conducting sensory impulses, maintaining water and electrolyte balance, and protecting against UV rays, radiation, environmental hazards, and infections.^{1,2} Skin injuries can result from trauma, burns, surgery, or complications from diseases like diabetes. The wound healing process, a complex regeneration activity involving inflammation, proliferation, and remodeling, may be compromised by factors such as repeated trauma, constant stress, infection, ischemia, and localized or systemic diseases, potentially leading to scarring or failure to heal.^{3,4} Although autologous skin grafting is considered the best treatment for severe dermal injuries, it is limited by the availability of donor tissues. Alternative treatments, like dermal substitutes, face challenges such as high costs, limited efficacy, and the inability to renew skin appendages.⁵ Consequently, there is a critical need to develop safer and more effective treatments for skin injuries. Advancements in medical science have led to the development of numerous techniques for the treatment of skin injuries.⁶⁻⁹

Mesenchymal stem cells (MSCs) are characterized by their abilities for self-renewal, multi-differentiation, and immune regulation,¹⁰ making them promising candidates for cell therapy.^{11,12} MSCs contribute to nearly all stages of the wound healing process, including inhibiting infection,¹³ promoting collagen deposition,¹⁴ enhancing wound contraction,¹⁵ stimulating angiogenesis,¹⁶ regenerating skin appendages, and boosting the growth of epidermal cells.¹⁷ However, MSC therapy can

encounter challenges such as low cell survival rates, the risk of immune rejection, and potential tumor formation. Notably, the paracrine factors released by MSCs are crucial to their therapeutic effect in wound healing.^{18,19} In this context, exosomes, the paracrine products of MSCs, have gained significant attention. These exosomes retain the beneficial functions of their parent cells while mitigating the associated risks. Research has shown that MSC-derived exosomes (MSC-Exo) enhance wound healing by inducing macrophage polarization to the M2 type,²⁰ regulating pro-inflammatory factors and chemokine expression,²¹ promoting cellular proliferation, migration, and vascularization, and modulating collagen dynamics to prevent excessive deposition and promote hydrolysis, thus reducing scar formation.²²

MicroRNAs (miRNAs) within the exosomes of MSCs play a critical role in skin healing. These miRNAs enhance cell proliferation,²³ modulate inflammatory responses,²⁴ promote angiogenesis,^{25,26} and mitigate scar formation²⁷ by intricately regulating signaling pathways and gene expression. This modulatory effect significantly improves the repair and rejuvenation of damaged skin tissue, positioning miRNAs in MSC exosomes as a promising therapeutic avenue for a broad spectrum of skin injuries and diseases.

Deer antlers are unique among mammalian accessory organs because they can fully regenerate periodically. This regeneration process is rapid during late spring and summer, slows in early autumn, and ossifies in late autumn. The ossified antlers will completely fall off in the next spring, and then the next cycle will begin.^{28–31} After antlers are shed, a wound approximately 45 millimeters in diameter forms but heals completely within 10 days, typically without scarring.³² The swift and scarless healing of deer antler wounds is closely associated with antler mesenchymal stem cells (AMSC).³³ Studies have demonstrated that injections of deer antler stem cells can effectively treat skin radiation damage by delaying onset, shortening healing time, and improving the quality of healing.³⁴ Conditioned medium from AMSC also promotes scarless repair of full-thickness skin injuries in rats,³⁵ with exosomes likely playing a crucial role in this process.

Herein, this study aimed to explore the treatment of skin wound healing by exosomes from AMSC (AMSC-Exo). The results had shown that AMSC-Exo significantly enhanced cell proliferation, migration, and angiogenesis *in vitro*, and expedited the healing of full-thickness skin wounds in mice. These effects were mediated through the regulation of collagen deposition and transformation of collagen fiber types. Through miRNA sequencing of AMSC-Exo, pivotal miRNAs and their signaling pathways were identified. The miR-21-5p/STAT3 signaling pathway was found to facilitate the communication between AMSC-Exo and keratinocyte cells, suggesting a promising approach for exosome-based therapies in skin wound healing.

Materials and Methods

Isolation and Culture of AMSC

All primary cell collections and animal experiments in this study were approved by the Animal Administration and Ethics Committee of the Institute of Special Animal and Plant Sciences of Chinese Academy of Agricultural Sciences (Approval Number: ISAPSAEC-2023-034D). A 4-year-old male sika deer (*Cervus nippon*) was selected from Dongda sika deer farm. When the deer antler had grown for approximately 45 days, the antler removal procedure was carried out in accordance with the regulations set by industry standards. The distal 5 cm of the tip tissue of the deer antler was cut and longitudinally sliced, and the mesenchymal layer was isolated as described in the previous report.³⁶ The mesenchymal layer was minced, and then digested with collagenaseII (Gibco, USA) at 37°C water bath with continuous shaking. Upon the observation of “burrs” forming at the edges, centrifugation at 1000 rpm for a duration of 5 min was conducted to remove the collagenase to obtain the AMSC. AMSC were cultured with DMEM/F12 supplemented with 10% FBS (PAN, DE) and 1% of penicillin-streptomycin (Gibco, USA) in a humidified incubator containing 5% (v/v) CO₂ at 37°C. The culture medium was replaced every other day.

The Identification of AMSC

The AMSC at 3–5 passages were identified by testing typical MSCs marker proteins (CD44, CD90) through both flow cytometry and immunofluorescence staining. Each well of a 12-well plate was inoculated with 1×10^5 AMSC cells. Upon reaching 80% confluence, the cells were fixed with 4% paraformaldehyde (Aldrich, USA) at room temperature for 15 min, followed by three times wash with PBS (Gibco, USA). Subsequently, the cells were blocked with 5% BSA (Yuanye, China) for 30 min. The cells were immunostained with CD44 (1:200, Proteintech, China) and CD90 (1:200,

Bioss, China) antibodies overnight at 4°C. The cells were washed 3 times with PBS. They were further incubated with fluorescein-conjugated secondary antibody (1:500, TransGen, China) in darkness at room temperature for 1 h, followed by three times wash with PBS. For immunofluorescence analysis, DAPI (Solarbio, China) was used to visualize the nuclei. Images were captured using a fluorescence microscope (Nikon, Japan). For flow cytometry (BD, USA), the immunostained AMSC were harvested, and filtered through a 40 µm filter prior to testing. At least 10000 cells were detected.

For further characterization of MSCs, their differentiation capabilities were investigated. In 6-well plates, a seeding density of 3×10^5 cells per well was utilized, and differentiation protocols were initiated once cells reached 90% confluence. Lipogenic induction medium (comprising dexamethasone 0.25 µM, rosiglitazone 1 µM, IBMX 0.5 mM, and insulin 5 µg/mL), osteogenic induction medium (containing sodium β-glycerophosphate 10 mM, dexamethasone 0.1 µM, and vitamin C 50 mg/L), and chondrogenic induction medium (with TGF-β1 10 ng/mL, dexamethasone 0.1 µM, vitamin C 50 µM, and insulin 6.25 µg/mL) were applied individually for a duration of 2 to 3 weeks. Subsequently, staining was performed using oil red O (Solarbio, China), alizarin red (Biotime, China), and Alcian blue (Solarbio, China) solutions, respectively. Images were captured using a fluorescence microscope (Nikon, Japan).

The Isolation of AMSC-Exo

The AMSC were cultured in DMEM/F12 supplemented with exosomes-depleted FBS (PAN, Germany) for 24 h. The conditioned medium was collected and underwent differential ultracentrifugation at 4°C with the following steps: 300 g for 10 min to remove the dead cells, 2000 g for 30 min to remove the cellular debris, 10,000 g for another 30 min to eliminate large extracellular vesicles. After filtrated with a 0.22-µm filter (Millipore, Burlington, MA), the filtrate underwent ultracentrifugation at 120,000 g for 120 min at 4°C using an ultracentrifuge (Beckman Coulter, USA). The pellet was resuspended in PBS and then ultracentrifuged again at 120,000 g for 90 min. Finally, the obtained AMSC-Exo was resuspended in PBS followed by stored at -80°C for further use.³⁷

The Characterization of AMSC-Exo

The morphologies of exosomes were characterized using transmission electron microscopy (JEOL, Tokyo, Japan). Particle size and concentration were determined through nanoflow cytometry (NanoFCM, Xiamen, China). Size distribution and zeta potential were assessed using a nanocoulter counter (Resuntech Co. LTD, Shenzhen, China) based on the resistive pulse sensing (RPS) method. Nanopore chips with a measuring range of 60–200 nm was selected in our experiment. The concentration of exosomal protein was quantified with the BCA protein detection kit (Thermo Scientific, USA). Immunoblotting was performed to detect the expression of known exosomal marker CD81 (1:1000, Abcam, USA), ALIX (1:1000, Abcam, USA), TSG101 (1:1000, Abcam, USA), and Golgi marker GM130 (1:5000, Abcam, USA).

Cell Viability Assay

The cellular proliferation and activity were assessed using a CCK-8 assay. HaCaT cells were seeded at a density of 3×10^3 cells/well in 96-well plates. AMSC-Exo with concentration of 8, 16, 32, 64, 128, and 256 µg/mL was added to the cells. After 72 h incubation, 10 µL of CCK-8 solution was added to each well and incubated at 37°C for another 2 h. The absorbance at 450 nm was measured using a microplate reader (BioTec, USA).

In vitro Wound-Healing Assay for Migration Ability

Wound-healing assays in vitro were performed to assess HaCaT cell migration in 24-well plates. The cells were seeded at a density of 3×10^5 cells per well. Once the cultured cell layer converged, a scratch was made along the diameter of the well using a 1 mL pipette tip. The wells were then washed three times with PBS to remove cell debris. Subsequently, 1 mL of serum-free DMEM-high-glucose medium was added to each well, along with 100 µg/mL of AMSC-Exo or an equal volume of PBS in separate wells. The scratch in each well was monitored and imaged using a fluorescence microscope (Nikon, Japan) at 0 and 12 h. The scratch area was quantified using Image J software.

Transwell Migration Assay

For the transwell assay, 3×10^4 HUVEC cells per well in serum-free medium were seeded into the upper chamber of the transwell 24-well plates (8 μm pore filters, Labselect, China). 600 μL medium containing 20% FBS was added to the lower chamber, then the cells were co-cultured overnight at 37°C. AMSC-Exo at a final concentration of 100 $\mu\text{g}/\text{mL}$ or equal volume of PBS was added to the lower chamber and cultured for 24 h. Subsequently, the cells attached to the upper surface of the filter membranes were carefully wiped clean with a cotton swab. The migrated cells on the lower surface were fixed with 4% paraformaldehyde for 15 min followed by staining with crystal violet. Images were captured using a microscope.

Tubular Formation Test

Matrigel (Corning, USA) were stored at -20°C and then dissolved overnight at 4°C. The 96-well plates and pipette tips were pre-cooled on ice for 30 min. A volume of 50 μL of matrigel matrix was evenly dispensed into each well of the 96-well plate and left to solidify at 37°C for 1 h. HUVEC cells were seeded into the matrigel at a density of 1×10^4 cells per well and cultured in a 5% CO_2 incubator at 37°C. Images were acquired at intervals of 3 h, and the results were analyzed using Image J software.

Establishment of Mouse Skin Trauma Model

ICR mice (12 weeks, male, about 40 g) were purchased from Shenyang Changsheng Biotechnology Company (Shenyang, China). All animals experiments were conducted in compliance with the guidelines and regulations and approved by the Animal Administration and Ethics Committee of the Institute of Special Animal and Plant Sciences, Chinese Academy of Agricultural Sciences (NO. ISAPSAEC-2023-034D). All the mice were raised in the standard condition with free access to water and food and 12 h dark/light cycle. The mice were anesthetized using 0.1 mL of 10% chloral hydrate. Subsequently, the dorsal skin was depilated, and a square full-thickness skin wound with a side length of 1.5 cm. The mice were then randomly divided into three groups ($n=5$): Control group: untreated. Gel group: treated with 100 μL hyaluronic acid gel. G-Exo (Gel-Exo) group: treated with 100 μL of hyaluronic acid gel containing 100 μg AMSC-Exo. The wounds of the mice in the Gel Group and G-Exo Group were treated with the respective gel daily. The skin injury sites were imaged every three days. The wound area ratios (%) = Area of residual wound / Area of initial wound \times 100%. On the 29th day, the mice were humanely euthanized, and the healing tissue from the center of the wound was collected for histological analysis.

Histological Assessment

The whole skin samples of the wound were fixed in 4% polyformaldehyde solution, embedded in paraffin and then sliced to 5 μm thick tissue sections. The pathological changes in the tissues were examined by hematoxylin and eosin (H&E) staining. The collagen deposition in the skin was determined using Masson's trichrome staining.

Immunohistochemistry

For immunohistochemical staining, the tissue sections were dewaxed and rehydrated, then blocked with goat serum for 30 min at 37°C. Primary antibodies CD31 (1:2000, Abcam, USA), COL1 (1:8000, Servicebio, China) and COL3 (1: 200, Boster, China) were incubated overnight at 4°C. Horseradish peroxidase (1:2000, Abcam, USA) was introduced and incubated in a light-protected environment at room temperature for 50 min. Diaminobenzamidine was utilized for chromogenic development, followed by a 5-min restaining with hematoxylin. Five random fields per section near the wound edges were counted by ImageJ software.

Luciferase Reporter Assay

The luciferase reporter plasmids containing wild-type (WT) or mutant (MUT) STAT3 3'-UTR were co-transfected into HaCaT cells with miR-21-5p mimic or a control miRNA. After 24 h of transfection, a luciferase assay was performed using the Dual Luciferase Reporter Assay System (Promega, USA) following to the manufacturer's instruction.

Western Blot

Cell lysis was performed using RIPA lysis buffer, followed by determination of total protein concentrations with the BCA assay kit. Equal protein amounts were then loaded onto 10% SDS-PAGE gels (Epizyme Biomedical Technology, Shanghai, China) for electrophoretic separation at 150 V for 80 min. Subsequently, proteins were transferred onto PVDF membranes and blocked with 5% non-fat milk in TBST for 1 h at room temperature. Next, the membranes were exposed to primary antibodies against CD81, TSG101, ALIX, GM130, MMP1, STAT3, TIMP3, and GAPDH (Abcam, USA) diluted in 5% BSA in TBST overnight at 4°C. After three washes with TBST, the membranes were incubated with horseradish peroxidase (HRP)-conjugated secondary antibodies (Thermo Fisher, USA) for 1 h at room temperature. Finally, protein signals were detected using a chemiluminescence kit (Thermo Fisher, USA) and imaged with a multifunctional imaging system (Tanon, Shanghai, China).

Statistical Analysis

Statistical analysis was performed using GraphPad Prism 6 software. Data were expressed as mean \pm standard deviation (SD), one-way ANOVA was used for comparison between different groups and the *t*-test was used for the comparison of the two sample means. $P < 0.05$ were considered as statistical significance.

Results

The Characterization of AMSC

The tip of the deer antler is anatomically segmented into distinct layers including the dermis, reserve mesenchymal (RM) layer, prechondroblast layer, transition zone, and cartilage layer, arranged sequentially from top to bottom.³⁶ The RM layer, situated beneath the dermal connective tissue (Figure 1A), exhibits a thickness ranging from 2–3 mm. It possesses a translucent, gel-like appearance when illuminated, and notably lacks of vascular network. As the growth center of the antler, the RM layer plays a pivotal role in facilitating the rapid antler growth process.

AMSC were successfully isolated and identified by cell morphology, surface marker proteins, and multi-lineage differentiation potential. AMSC displayed typical fibroblast-like morphology, featuring elongated spindle-shaped bodies with discernible vortex formations and strong adherence properties (Figure 1B). Immunofluorescence staining of AMSC demonstrated positive expression of CD44 and CD90 (Figure 1C), which are surface markers commonly associated with MSCs. Flow cytometry analysis further confirmed high expression levels of CD44 (97.4%) and CD90 (97.3%) in AMSC (Figure 1D), indicating their MSC characteristics.

MSCs have the potential to differentiate into (mesoderm-derived cells) osteoblasts, adipocytes and chondrocytes *in vitro*. Multidirectional differentiation potential of MSCs is an important indicator to determine the characteristics of stem cells. In this study, multidirectional differentiation induction was performed on the isolated AMSC. Following induction with lipid induction medium for 2 weeks and subsequent staining with oil red O, abundant orange-red lipid droplets were observed (Figure 1E), indicative of adipogenic differentiation. Moreover, after 3 weeks of culture in osteogenic induction medium and staining with alizarin red, conspicuous bright red calcium nodules were discernible to the naked eye (Figure 1F), demonstrating osteogenic differentiation. Additionally, after 3 weeks of chondrogenic induction medium culture and staining with alcian blue, distinct bright blue proteoglycans were evident, confirming the chondrogenic potential of AMSC (Figure 1G). These findings collectively suggest that AMSC possess the capability for adipogenic, osteogenic, and chondrogenic differentiation *in vitro*.

The Characterization of AMSC-Exo

AMSC-Exo were obtained through ultracentrifugation, followed by characterization of their morphology, particle size, concentration, and specific protein expression using transmission electron microscopy, nanoflow cytometry, nanocoulter counter, and western blotting. Transmission electron microscopy revealed that the isolated AMSC-Exo exhibited typical vesicular structures, with an estimated particle size of approximately 150 nm (Figure 2A). Western blot analysis confirmed the expression of key marker proteins in AMSC-Exo. Specifically, CD81, TSG101, and ALIX proteins were detected, while the negative marker GM130 was absent (Figure 2B). These results indicate the high purity of the obtained AMSC-Exo.

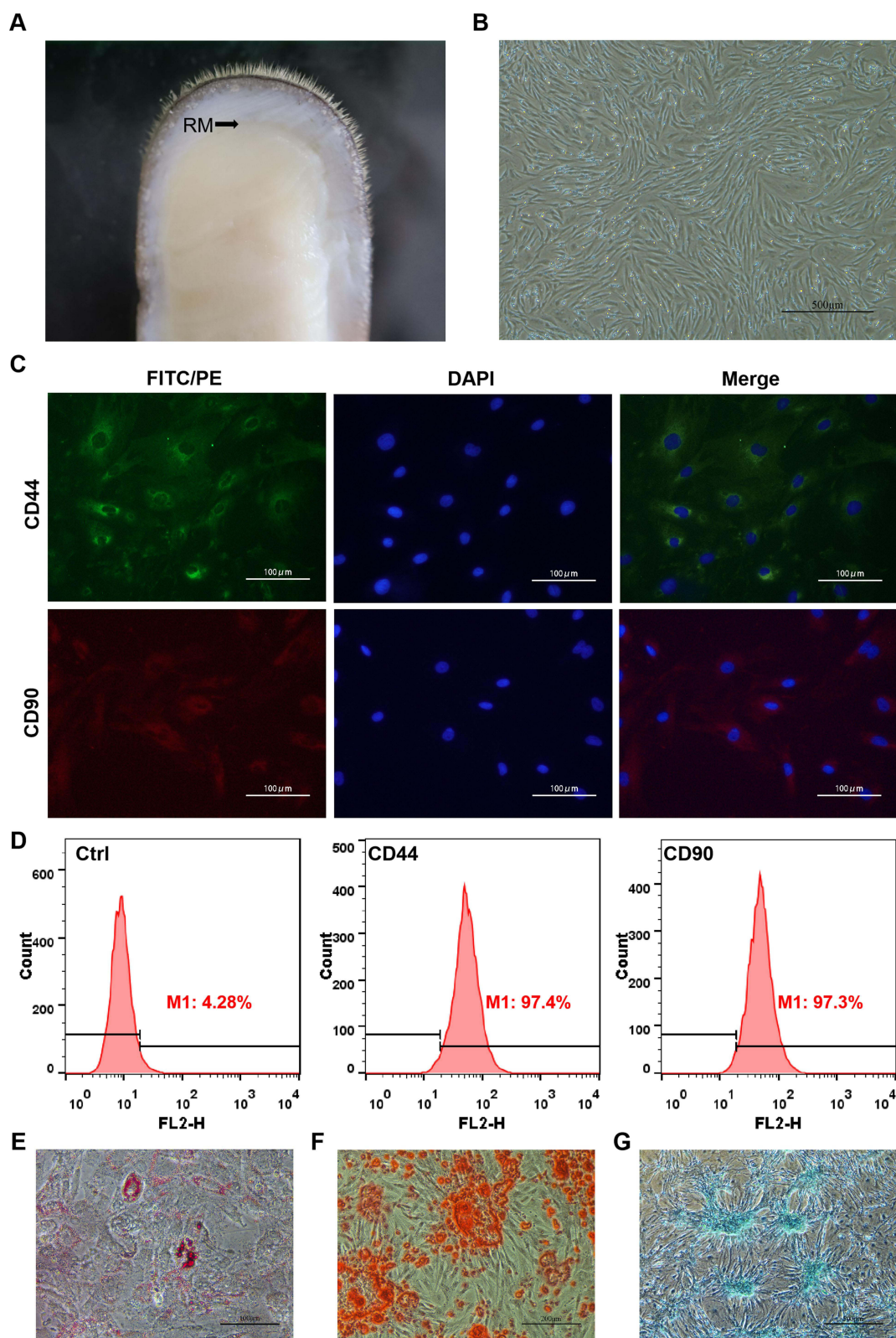


Figure 1 Isolation and identification of the AMSC. **(A)** The tip of velvet antler, black arrow indicates the reserve mesenchymal layer. **(B)** Optical morphology of AMSC under light field microscope, scale bars: 500 μ m. The expressions of AMSC surface markers CD44 and CD90 identified by immunofluorescence staining **(C)** and flow cytometry **(D)**, scale bar: 100 μ m. Adipogenic, osteogenic and chondrogenic differentiation potentials of AMSC examined by oil red O **(E)**, scale bar: 100 μ m, alizarin red **(F)**, scale bar: 200 μ m and alcian blue staining **(G)**, scale bar: 500 μ m.

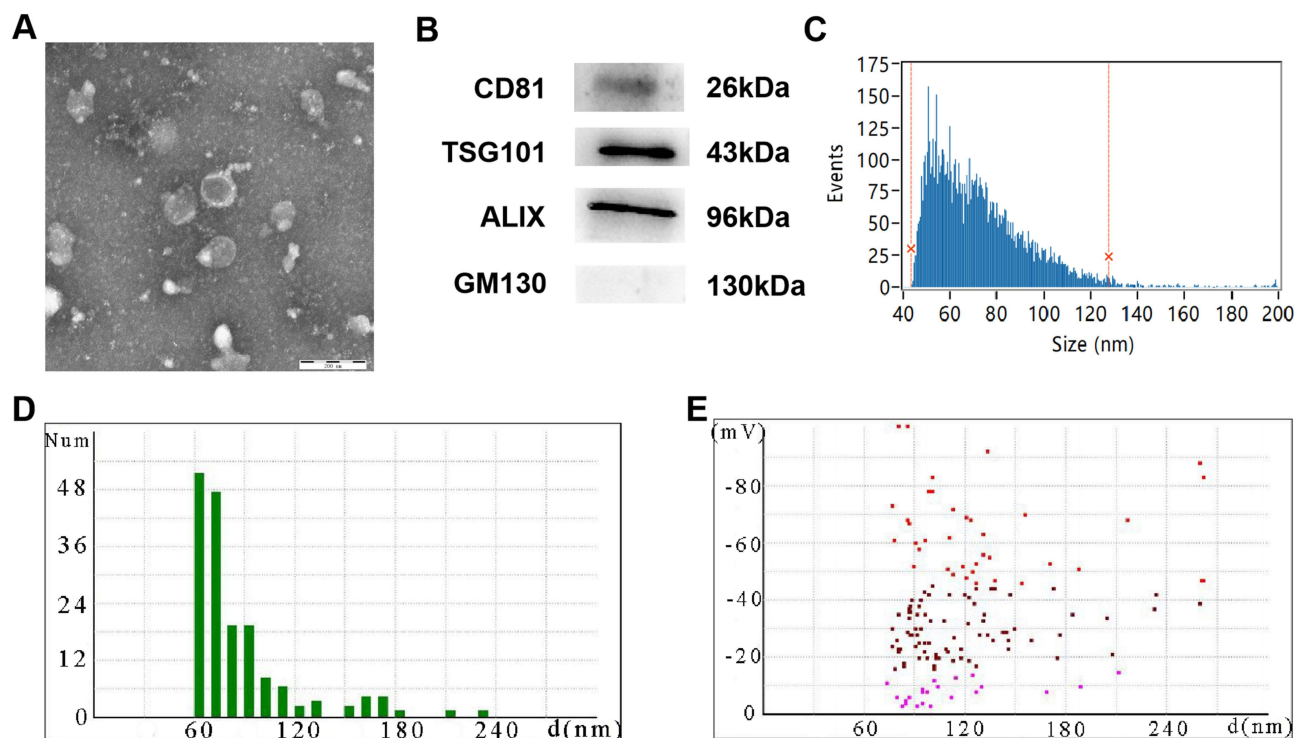


Figure 2 The characterization of AMSC-Exo. (A) TEM image of AMSC-Exo, scale bar: 200 nm. (B) Immunoblot analysis of known exosomal markers (CD81, TSG101 and ALIX) and negative marker (GM130) in AMSC-Exo. The particle size distribution of AMSC-Exo detected by nanoflow cytometry (C) and nanocoulter counter (D). (E) The zeta potential of AMSC-Exo measured by nanocoulter counter.

Nanoflow detection is a quantitative characterization technique of single-particle nanoparticles based on sheath flow single molecule fluorescence technology, which covers the detection blind area below 200 nm of traditional flow cytometry. Nanoflow cytometry results confirmed that 98% of the particles fell within the range of 43 to 127 nm, with an average particle size of 71 nm (Figure 2C). Additionally, the particle size distribution and zeta potential of AMSC-Exo was further evaluated using nanocoulter counter. The findings revealed an average particle size of 72 nm (Figure 2D), closely aligning with the results obtained from nanoflow cytometry. Zeta potential is an important indicator to evaluate the stability of nanoparticles reflecting the number of net charges on the surface of the particles. The more net charges, the greater the electrostatic repulsion and the more stable in the system. As proved in Figure 2E, the zeta potential of the AMSC-Exo was -35 mV, indicating that the AMSC-Exo had good stability.

Effects of AMSC-Exo on Cell Proliferation, Migration and Tubule Formation

To investigate the biological functions of AMSC-Exo in wound repair, several experiments were conducted. Initially, the proliferation of HaCaT cells was assessed using the Cell Counting Kit-8 (CCK-8) assay. The results indicated that AMSC-Exo at concentrations of 64 and 128 $\mu\text{g}/\text{mL}$ significantly increased HaCaT cell proliferation (Figure 3A). The role of AMSC-Exo in cell migration was also explored, which is critical for effective tissue repair. Scratch and transwell migration assays were performed to evaluate the migration of HaCaT keratinocyte cells and HUVEC endothelial cells, respectively. The scratch assay showed that AMSC-Exo treatment led to a significantly reduced scratch area compared to the untreated group, suggesting enhanced migration of HaCaT cells (Figure 3B and C). Further, the transwell assays demonstrated that HUVEC cells exposed to AMSC-Exo exhibited increased migratory capabilities (Figure 3D and E). These findings collectively suggested that AMSC-Exo promotes the proliferation and migration of both epidermal and endothelial cells, likely through a paracrine mechanism.

Angiogenesis plays a vital role in wound repair. To evaluate this process, we assessed endothelial cell tubule formation using Matrigel, a well-established in vitro assay that measures the ability of endothelial cells to form blood vessels by analyzing tubule length and the number of nodes and branches. In this assay, HUVEC cells treated with

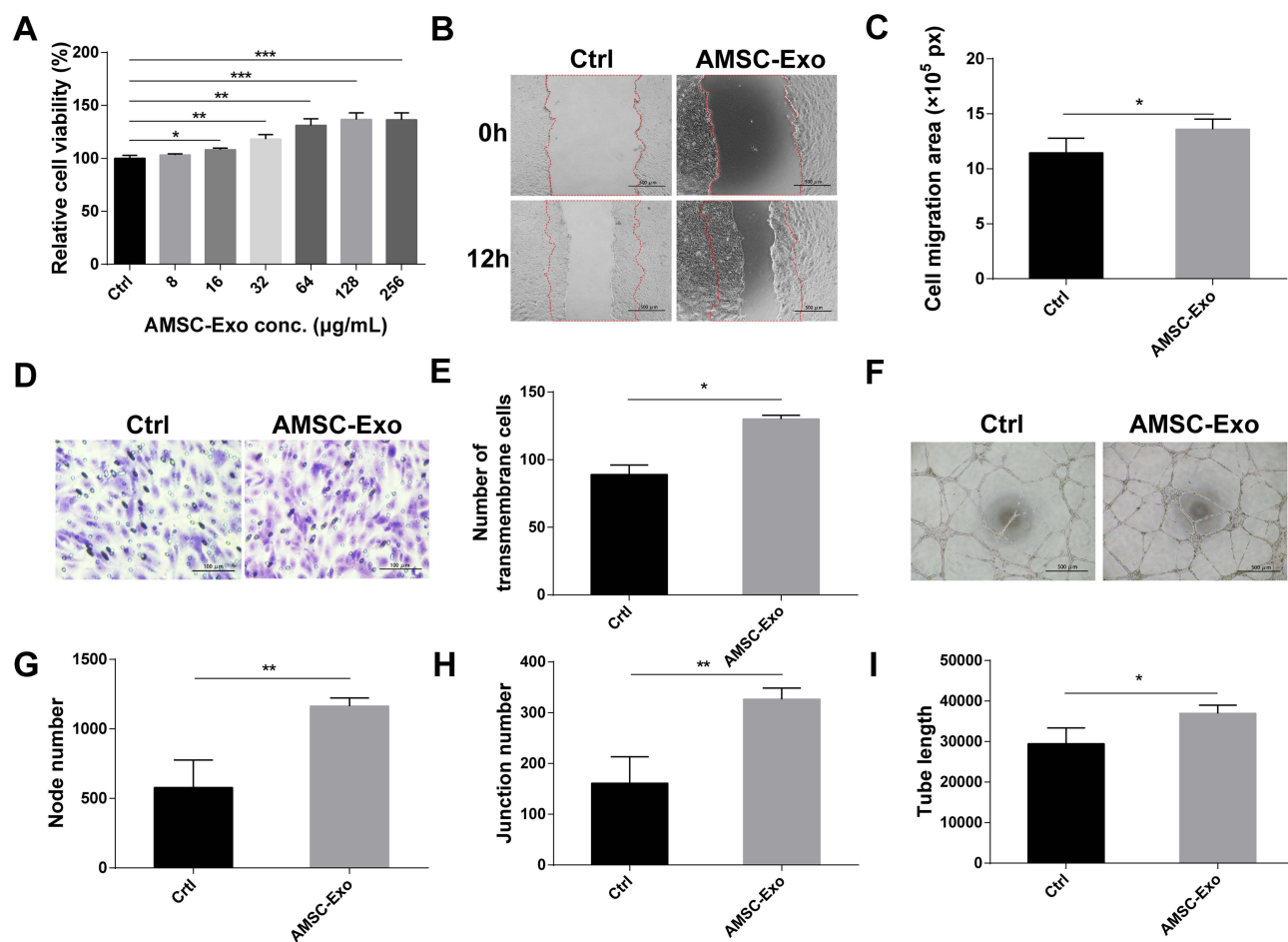


Figure 3 Effects of AMSC-Exo on cell proliferation, migration and tubule formation. **(A)** The cell viability of HaCaT cells after 72 h treatment with AMSC-Exo. **(B)** HaCaT cell migration was detected by scratch assay, scale bar: 500 μm . **(C)** Cell migration area was counted. **(D)** HUVEC cell migration was detected by transwell, scale bar: 100 μm . **(E)** HUVEC transmembrane cell number was counted. **(F)** The tube formation of HUVEC, scale bar: 500 μm . HUVEC tubule formation node **(G)**, junction number **(H)** and tube length **(I)**. In the picture *Means $p < 0.05$, **Means $p < 0.005$, and ***Means $p < 0.001$.

AMSC-Exo showed significantly enhanced formation of tubule networks compared to the control group. Specifically, the number of nodes and branches in the AMSC-Exo group was twice that observed in the control group, and the tubule lengths were 1.25 times longer (Figure 3F–I). These results demonstrate that AMSC-Exo effectively promotes tubule formation and facilitates angiogenesis, thereby confirming its potential to support healing processes in vitro.

AMSC-Exo Stimulates Full-Thickness Skin Wound Healing in Mice

To evaluate the therapeutic efficacy of AMSC-Exo in wound healing, a full-thickness skin wound model was established in mice. Each mouse was subjected to a 1.5cm x 1.5cm square full-layer skin defect on the back. The mice were then randomly assigned to one of three groups: a control group receiving no treatment, a group treated with hydrogel only (Gel group), and a group treated with hydrogel containing AMSC-Exo (G-Exo group). Both the Gel and G-Exo groups received daily applications of their respective treatments (Figure 4A). The wounds were photographed every three days to monitor healing progress. As shown in Figure 4B, all wounds initially developed sizable scabs, with the surrounding scab appearing pale yellow—a sign of inflammation in the early stages of wound healing. The G-Exo group exhibited the fastest wound closure rate, with significant healing observed from day 7 and nearly complete closure by day 16. Upon complete clearance of the scab, the wound area exhibited darkening and pigmentation in contrast to the adjacent healthy skin. Statistical analysis of the wound area ratios from day 29 to day 0 (Figure 4C) revealed that the G-Exo group had the smallest ratio, indicating the most significant reduction in wound size. These findings demonstrate that AMSC-Exo significantly enhances the repair process in full-thickness skin defects in mice, promoting more rapid and effective wound closure.

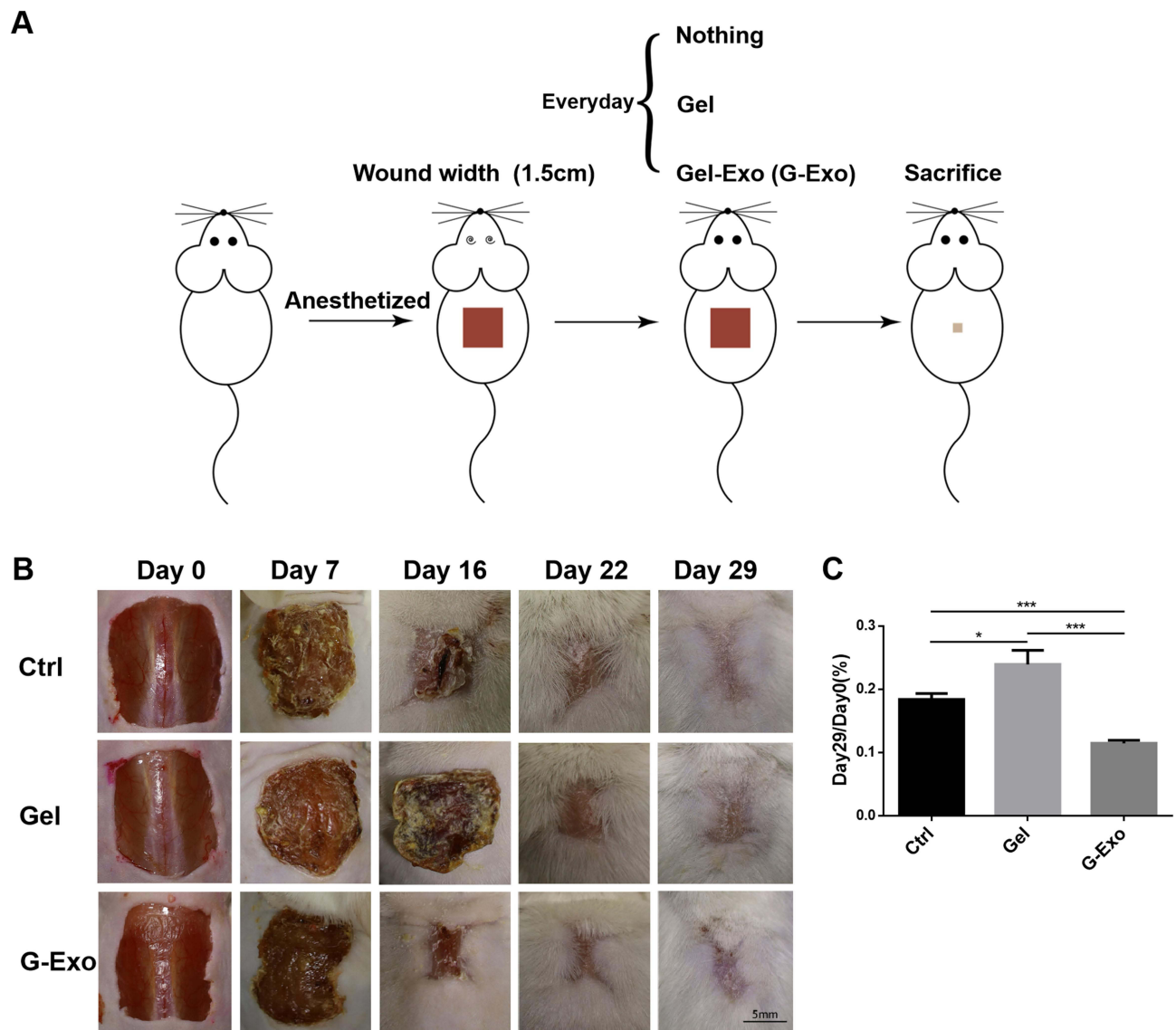


Figure 4 The effect of AMSC-Exo on wound healing in a mouse full-thickness skin injury model. **(A)** Experimental procedure of the mice. **(B)** Global morphological photographs of wound area treated with PBS (Ctrl), gel (Gel) or gel-AMSC-Exo (G-Exo) on day 0, 7, 16, 22, 29, scale bar: 5 mm. **(C)** Wound area ratios of day 29 to day 0. In the picture *Means $p < 0.05$ and ***Means $p < 0.001$.

AMSC-Exo Improve the Skin Wound Healing Quality of Mice

To further assess the repair capabilities of AMSC-Exo, immunohistochemical staining was conducted on the healed tissues. On the 29th day post-injury, after euthanizing the mice, skin samples were collected from both the wound site and surrounding areas. Hematoxylin and eosin (H&E) staining highlighted a clear demarcation between the epidermis and dermis in the G-Exo group, contrasting with the control and Gel treated groups, as shown in [Figure 5A](#). Notably, the epidermis in the G-Exo group maintained a well-preserved structure with three distinct layers of cells, measuring an average thickness of $27.4 \pm 5.1 \mu\text{m}$, similar to that of healthy mice skin ($25 \mu\text{m}$), and considerably thinner than in the control group ($42.0 \pm 7.1 \mu\text{m}$) and Gel group ($77.4 \pm 16.6 \mu\text{m}$) ([Figure 5B](#)). The abnormal thickening of epidermis in the gel group may be caused by excessive collagen deposition during scar healing. Further examination using Masson's trichrome staining showed that the dermal layer in the G-Exo group contained densely packed, well-organized collagen fibers, unlike the less structured arrangement seen in the control and gel treated groups. Moreover, CD31 immunostaining indicated enhanced angiogenesis in the G-Exo group, with a significantly higher number of blood vessels (74 ± 10) compared to the control (49 ± 3) and Gel treated groups (42 ± 4) ([Figure 5C](#)). These results suggest that AMSC-Exo not

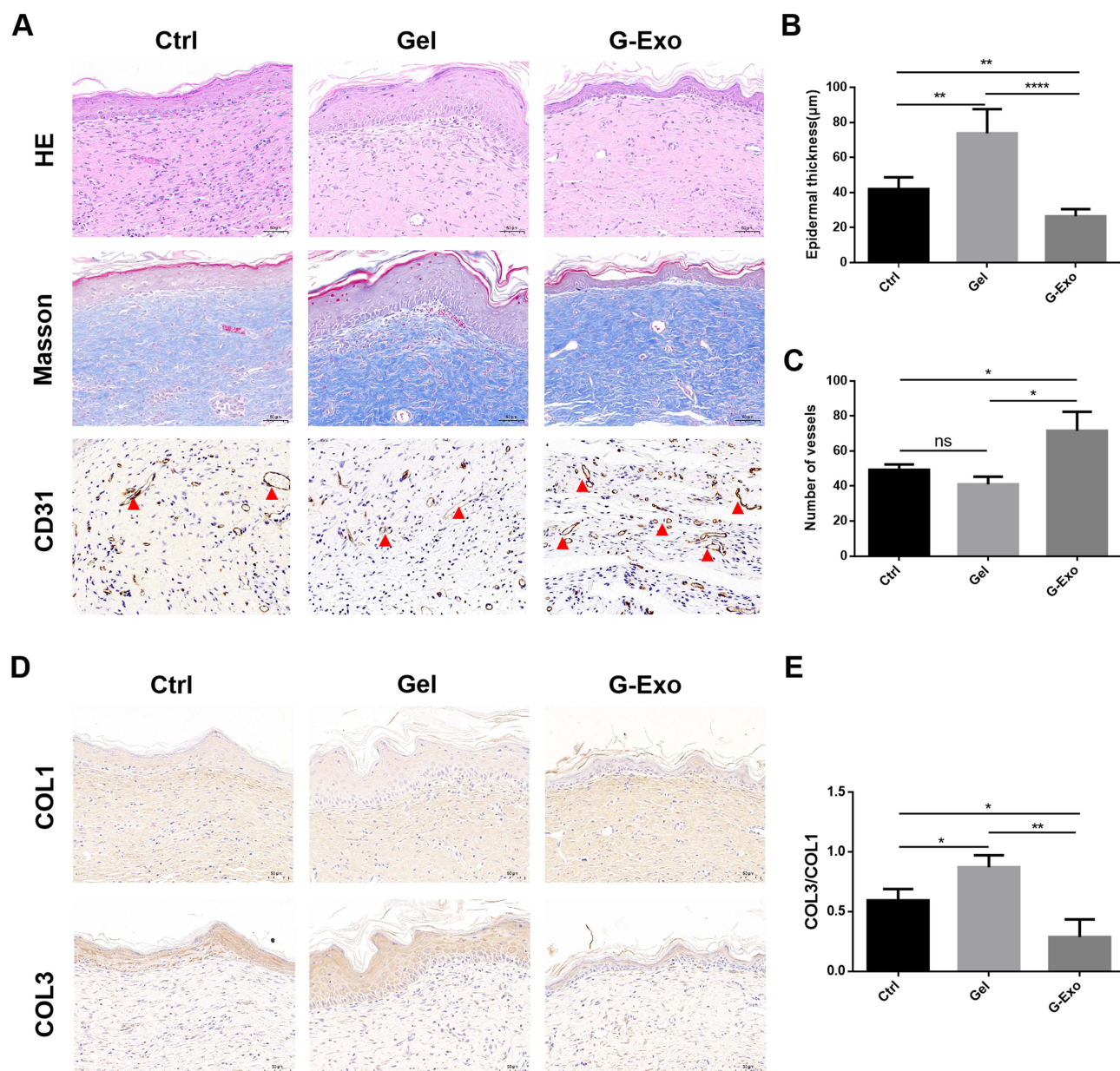


Figure 5 AMSC-Exo improved the healing quality of back wound in mice. **(A)** Representative images of H&E, Masson's trichrome staining and CD31 immunohistochemistry of the skin sections of day 29 in Ctrl group, Gel group or G-Exo group. The red triangles indicate the CD31 positive expression of new blood vessels, scale bar: 50 µm. **(B)** Quantitative analysis of the thickness of newly formed epidermis. **(C)** Number of CD31 positive stained vessels. **(D)** COL1 and COL3 immunohistochemical staining of the sections on day 29 after different treatments, scale bar: 50 µm. **(E)** Quantitative analysis of COL3 and COL1. In the picture *Means $p < 0.05$, **Means $p < 0.005$, and ***Means $p < 0.0001$.

only promotes more organized collagen fiber deposition but also enhances vascular formation, contributing to improved skin regeneration and reduced scarring in full-thickness skin wounds.

Collagen types I (COL 1) and III (COL 3) are the primary forms present in the extracellular matrix (ECM) of skin, each playing distinct roles in tissue structure and repair. COL 1, known for its thick fibers, forms a durable scaffold with a low turnover rate, providing structural integrity to the skin. Conversely, COL 3, which comprises thinner, less durable fibers, has a high turnover rate and is crucial during the initial stages of skin injury repair, facilitating rapid remodeling of damaged tissue. Typically, COL 1 levels surpass those of COL 3 in healthy skin. However, during the early phase of wound healing, the deposition of COL 3 predominates.³⁸ As healing progresses, collagen fibers transition from COL 3 to COL 1 during the maturation phase, enhancing tissue strength and flexibility through

The GO functional annotation categorized gene functions into three domains: biological process (BP), cellular component (CC), and molecular function (MF). Visualization of the results revealed the top attributes within each domain, highlighting that the most enriched BP terms included “cell division”, “cell cycle”, and “angiogenesis”, which are crucial for cell proliferation and the formation of new blood vessels (Figure 6B and C). These findings underscore the pivotal role of AMSC-Exo in promoting cell proliferation and angiogenesis, confirming observations from prior experimental results.

Further analysis using the KEGG database provided a systematic view of the gene networks influenced by these miRNAs. The top pathways identified were significantly associated with cell proliferation, including the Ras signaling pathway, Hippo pathway, PI3K-Akt pathway, and MAPK signaling pathway. Angiogenesis-related pathways, notably the HIF-1 signaling pathway and again the PI3K-Akt pathway, were also highlighted (Figure 6D). These pathways suggest that AMSC-Exo may regulate gene expression crucial for these processes, thereby enhancing the cellular activities necessary for effective wound healing.

STAT3 is the Direct Target of miR-21-5p

miR-21-5p, the predominant miRNA in AMSC-Exo, plays a crucial role in activating the PI3K/Akt and ERK1/2 signaling pathways by down-regulating the SPRY2 gene. This regulation promotes the proliferation and migration of HUVEC and HSF cells.⁴³ Suggesting that miR-21-5p is a key active component in these exosomes. To further understand the impact of miR-21-5p on skin healing, we analyzed its target genes using TargetScan, focusing on those with prediction scores above 90 (Figure 7A). One significant target, the signal transducer and activator of transcription 3

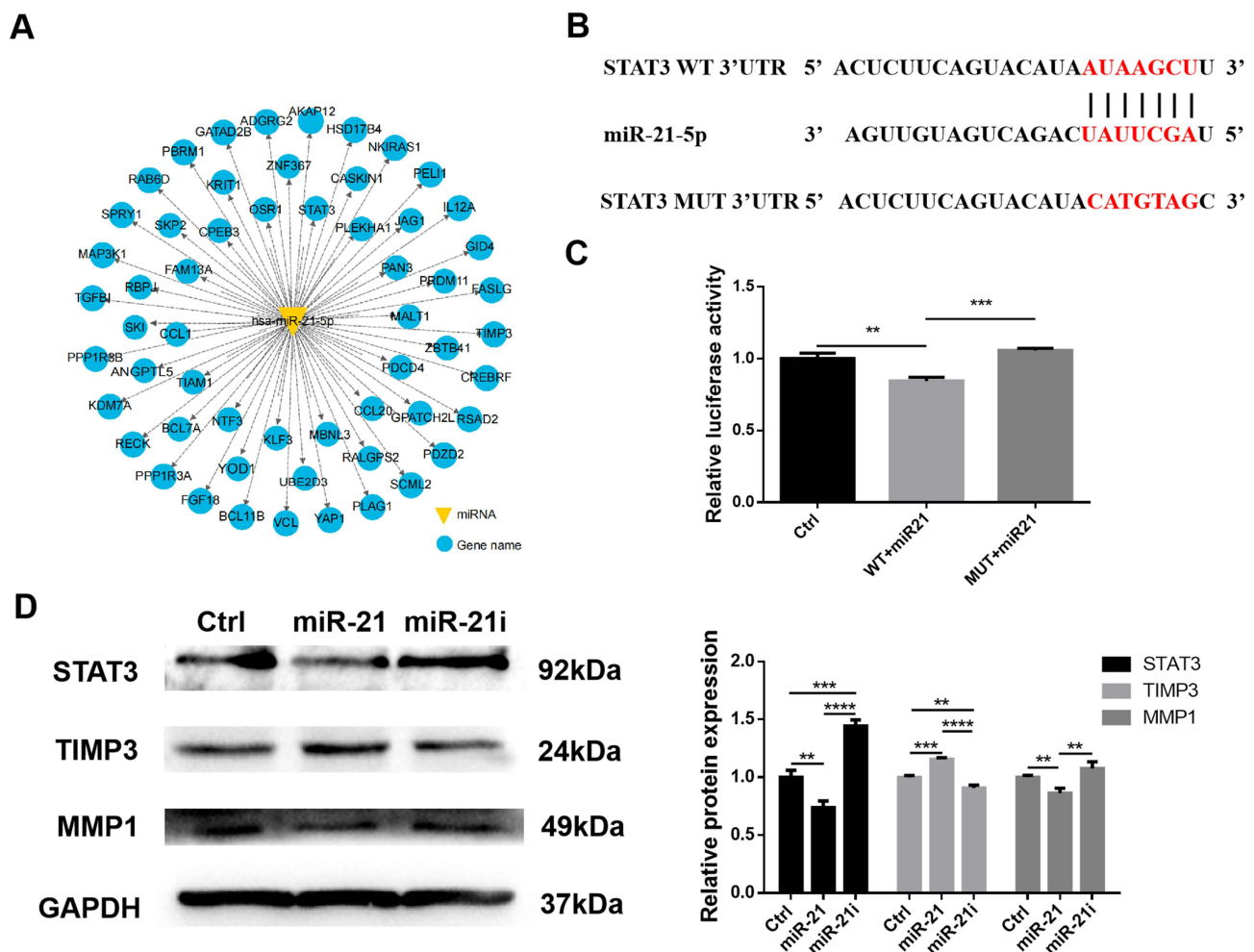


Figure 7 STAT3 is the direct target of miR-21-5p. (A) Prediction of miR-21-5p target genes by TargetScan. (B) The binding sites between miR-21-5p and STAT3. (C) Dual luciferase reporter gene analysis in HaCaT cells. (D) Relative protein expression of STAT3, TIMP3, MMP1 and GAPDH in HaCaT cells after miR-21-5p mimics (miR-21) or miR-21-5p inhibitor (miR-21i) treatment. In the picture **Means $p < 0.005$, and ***Means $p < 0.001$, ****Means $p < 0.0001$.

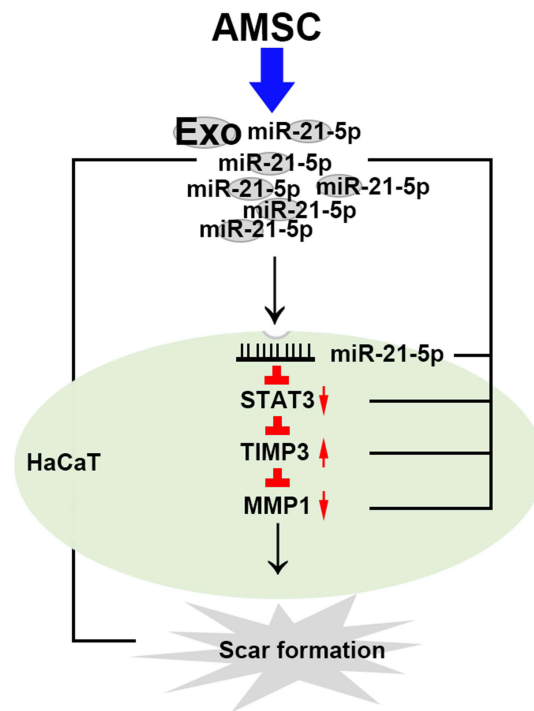


Figure 8 Schematic diagram of the experimental results.

(STAT3), was identified as critical, particularly for cell migration. Further analysis confirmed that miR-21-5p could bind to the 3'-UTR of STAT3, as demonstrated in a dual luciferase reporter gene system. This system was co-transfected with miR-21-5p mimics into HaCaT cells, and the results validated the binding of miR-21-5p to STAT3's 3'-UTR (Figure 7B). Subsequent assays showed that the luciferase activity associated with the wild type (WT) STAT3 decreased following transfection with miR-21-5p mimics, whereas the mutant (MUT) STAT3 remained unchanged, confirming the specificity of the interaction (Figure 7C). Further experiments revealed that treatment with miR-21-5p mimics led to a reduction in STAT3 and MMP1 gene expression levels, while increasing the expression of the TIMP3 gene in HaCaT cells, compared to control and miR-21i-treated cells (Figure 7D). These findings highlight the pivotal role of miR-21-5p in modulating gene expression that contributes to the enhanced healing properties of AMSC-Exo (summarized in Figure 8).

Discussion

Stem cell therapy, recognized as a novel treatment strategy for skin injuries, allows MSCs to differentiate into various cell types such as keratinocytes, endothelial cells, and fibroblasts.⁴⁴ Despite its potential, stem cell therapy faces significant limitations. Notably, the survival rate of transplanted stem cells is low, with less than 3% of mesenchymal stem cells integrating into target organs in models of heart, kidney, liver, and pancreas injuries.^{18,45–48} The harsh microenvironment of skin injuries, characterized by cell necrosis, inflammation, and low oxygen levels, further complicates the survival of MSCs. Studies tracking fluorescence-labeled bone marrow stem cells (BMSCs) have shown that these cells are depleted from wound sites within a week,⁴⁹ indicating transient presence rather than prolonged integration. Moreover, concerns exist regarding the consistency and stability of stem cell-based products, especially given the potential for xenogeneic stem cell rejection and long-term risks that may not be immediately apparent post-administration. The isolation and culture methods used for MSCs, which often involve animal serum, can expose cells to endotoxins, adding another layer of complexity to their clinical use.

Despite these issues, MSCs exhibit substantial therapeutic effects, mainly through paracrine actions rather than direct cell replacement.¹⁹ This understanding has shifted focus towards MSC-derived exosomes (MSC-Exo), which offer several advantages: smaller size, lower complexity, and absence of a nucleus, reducing the risk of tumor formation

and increasing stability and storage potential. They can also be engineered to deliver specific proteins, small molecules, or RNA directly to injury sites.⁵⁰

Among MSCs, AMSC are distinguished by their unique capability to repeatedly and completely regenerate antler tissue, showcasing rapid, scar-free healing not observed in other stem cell types. This exceptional regenerative ability underscores the potential of AMSC-Exo as an innovative and effective therapy for managing difficult-to-treat chronic wounds and enhancing post-surgical healing. Compared to conventional MSC sources, AMSC demonstrate superior efficacy in promoting rapid and scar-free wound repair, positioning their exosomes as a powerful option for decellularization therapies. The therapeutic effectiveness of AMSC-Exo is, at least in part, mediated by specific miRNAs, including miR-21-5p, among others. These miRNAs significantly influence crucial signaling pathways, including PI3K/Akt and MAPK, which are essential for promoting cell migration, angiogenesis, and collagen remodeling. The impact on these pathways confirms the significant potential of AMSC-Exo in regenerative medicine, making them a promising treatment option for improving wound healing and tissue regeneration.

This study demonstrates the significant therapeutic potential of AMSC-Exo in treating full-thickness skin injuries. AMSC-Exo facilitated the proliferation and migration of HaCaT keratinocyte cells and enhanced migration and tube formation in HUVEC endothelial cells, vital for effective wound healing. Additionally, treatment with G-Exo, a specific formulation of AMSC-Exo, resulted in increased skin healing rates, enhanced neovascularization, and accelerated collagen transition from type III to type I, leading to orderly collagen arrangement. Notably, the treated mice exhibited a complete, scar-free healing process, and the thickness of their new epidermis closely matched that of healthy skin. This was accompanied by a lack of skin appendages, possibly due to the influence of growth factors and cytokines from AMSC.

MiRNAs hold significant promise for disease treatment due to their ability to modulate gene expression, providing a powerful tool for therapeutic intervention.^{51,52} In our study, the excellent outcomes observed are linked to specific microRNAs present in AMSC-Exo, particularly miR-21-5p, miR-27b, miR-29a, miR-125b, and miR-155. These miRNAs regulate key signaling pathways, such as PI3K/Akt and MAPK, which are essential for controlling cell behavior and gene expression. For instance, miR-21^{53,54} promotes cell proliferation and migration by down-regulating VHL,⁵⁵ while miR-21-5p enhances these processes by targeting SPRY2⁴³ and supports angiogenesis and granulation through macrophage polarization towards the M2 phenotype.⁵⁶ It also boosts fibroblast migration by targeting RASA1, accelerating skin repair,⁵⁷ and regulates STAT3 and TIMP3 to reduce MMP1 production, curbing excessive cell migration and minimizing scar formation. Similarly, miR-27b promotes angiogenesis and skin repair by regulating VEGF-C expression and accelerates cutaneous wound healing through the E3 ubiquitin ligase ITCH pathway. Studies have shown that miR-27b enhances angiogenesis and skin regeneration in scalded rats by modulating VEGF-C levels, and extracellular vesicle-carried miR-27b from mesenchymal stem cells has been found to expedite wound healing by activating the ITCH pathway.^{58,59} These findings underscore the significant impact of AMSC-Exo on skin regeneration and highlight its potential as a novel therapeutic strategy for complex skin injuries.

Conclusion

In conclusion, our study utilized AMSC-Exo to treat skin wounds. We extracted exosomes from conditioned culture medium of AMSC (AMSC-Exo). The AMSC-Exo effectively promotes the proliferation and migration of HaCaT keratinocyte cells and enhances migration and tube formation in HUVEC endothelial cells. In the skin injury mice models, AMSC-Exo treatment improved the healing quality of skin in mice by stimulating angiogenesis, regulating extracellular matrix deposition, and promoting re-epithelialization. Notably, miR-21-5p within AMSC-Exo played a pivotal role by down-regulating STAT3 and activating TIMP3, which led to decreased MMP1 production and reduced scar formation. These findings highlight the promise of exosome-based therapies in utilizing antler stem cells' regenerative abilities to enhance skin repair and regeneration.

Acknowledgments

This work was funded by Jilin Province Science and Technology Development Plan Project (20220101274JC, 20210202030NC) and the Science and Technology Innovation Program of the Chinese Academy of Agricultural Sciences (No. CAAS-ASTIP-2021-ISAPS).

Author Contributions

All authors made a significant contribution to the work reported, whether that is in the conception, study design, execution, acquisition of data, analysis and interpretation, or in all these areas; took part in drafting, revising or critically reviewing the article; gave final approval of the version to be published; have agreed on the journal to which the article has been submitted; and agree to be accountable for all aspects of the work.

Disclosure

The authors report no conflicts of interest in this work.

References

1. Zouboulis CC, Makrantonaki E. Clinical aspects and molecular diagnostics of skin aging. *Clin Dermatol*. 2011;29(1):3–14. doi:10.1016/j.clindermatol.2010.07.001
2. Farage MA, Miller KW, Elsner P, et al. Characteristics of the aging skin. *Adv Wound Care*. 2013;2(1):5–10. doi:10.1089/wound.2011.0356
3. Li Q, Gong S, Yao W, et al. Exosome loaded genipin crosslinked hydrogel facilitates full thickness cutaneous wound healing in rat animal model. *Drug Delivery*. 2021;28(1):1.
4. Cha J, Falanga V. Stem cells in cutaneous wound healing. *Clin Dermatol*. 2007;25(1):73–78. doi:10.1016/j.clindermatol.2006.10.002
5. Burd A, Ahmed K, Lam S, et al. Stem cell strategies in burns care. *Burns*. 2007;33(3):282–291. doi:10.1016/j.burns.2006.08.031
6. Li C, Xiong Y, Fu Z, et al. The direct binding of bioactive peptide Andersonin-W1 to TLR4 expedites the healing of diabetic skin wounds. *Cell Mol Biol Lett*. 2024;29(1):24.
7. Li C, Fu Z, Jin T, et al. A frog peptide provides new strategies for the intervention against skin wound healing. *Cell Mol Biol Lett*. 2023;28(1):61. doi:10.1186/s11658-023-00468-3
8. Zhang X, Feng C, Wang S, et al. A novel amphibian-derived peptide alleviated ultraviolet B-induced photodamage in mice. *Biomed Pharmacother*. 2021;136:111258. doi:10.1016/j.biopha.2021.111258
9. Qin W, Liu K, Su H, et al. Tibial cortex transverse transport promotes ischemic diabetic foot ulcer healing via enhanced angiogenesis and inflammation modulation in a novel rat model. *Eur J Med Res*. 2024;29(1):155.
10. Chen Z, Jin M, He H, et al. Mesenchymal stem cells and macrophages and their interactions in tendon-bone healing. *J Orthop Translat*. 2023;39:63–73. doi:10.1016/j.jot.2022.12.005
11. Liu W, Yu M, Xie D, et al. Melatonin-stimulated MSC-derived exosomes improve diabetic wound healing through regulating macrophage M1 and M2 polarization by targeting the PTEN/AKT pathway. *Stem Cell Res Ther*. 2020;11(1):259.
12. Yang M, Sheng L, Zhang TR, et al. Stem cell therapy for lower extremity diabetic ulcers: where do we stand? *Biomed Res Int*. 2013;2013:462179. doi:10.1155/2013/462179
13. Krasnodembskaya A, Song Y, Fang X, et al. Antibacterial effect of human mesenchymal stem cells is mediated in part from secretion of the antimicrobial peptide LL-37. *Stem Cells*. 2010;28(12):2229–2238. doi:10.1002/stem.544
14. Fathke C, Wilson L, Hutter J, et al. Contribution of bone marrow-derived cells to skin: collagen deposition and wound repair. *Stem Cells*. 2004;22(5):812–822. doi:10.1634/stemcells.22-5-812
15. Neuss S, Schneider RK, Tietze L, et al. Secretion of fibrinolytic enzymes facilitates human mesenchymal stem cell invasion into fibrin clots. *Cells Tissues Organs*. 2010;191(1):36–46. doi:10.1159/000215579
16. Halkos ME, Zhao ZQ, Kerendi F, et al. Intravenous infusion of mesenchymal stem cells enhances regional perfusion and improves ventricular function in a porcine model of myocardial infarction. *Basic Res Cardiol*. 2008;103(6):525–536.
17. Nakagawa H, Akita S, Fukui M, et al. Human mesenchymal stem cells successfully improve skin-substitute wound healing. *Br J Dermatol*. 2005;153(1):29–36. doi:10.1111/j.1365-2133.2005.06554.x
18. Ochiai H, Kishi K, Kubota Y, et al. Transplanted mesenchymal stem cells are effective for skin regeneration in acute cutaneous wounds of pigs. *Regener Ther*. 2017;7:8–16. doi:10.1016/j.reth.2017.06.003
19. Phinney DG, Pittenger MF. Concise review: MSC-derived exosomes for cell-free therapy. *Stem Cells*. 2017;35(4):851–858. doi:10.1002/stem.2575
20. Heo JS, Choi Y, Kim HO, et al. Adipose-derived mesenchymal stem cells promote M2 macrophage phenotype through exosomes. *Stem Cells Internat*. 2019;2019:1–10.
21. Zhou Y, Zhao B, Zhang XL, et al. Combined topical and systemic administration with human adipose-derived mesenchymal stem cells (hADSC) and hADSC-derived exosomes markedly promoted cutaneous wound healing and regeneration. *Stem Cell Res Ther*. 2021;12(1):257. doi:10.1186/s13287-021-02287-9
22. Tutuianu R, Rosca A, Iacomi DM, et al. Human mesenchymal stromal cell-derived exosomes promote in vitro wound healing by modulating the biological properties of skin keratinocytes and fibroblasts and stimulating angiogenesis. *Int J Mol Sci*. 2021;22(12):6239. doi:10.3390/ijms22126239
23. Wei Q, Wang Y, Ma K, et al. Extracellular vesicles from human umbilical cord mesenchymal stem cells facilitate diabetic wound healing through MiR-17-5p-mediated enhancement of angiogenesis. *Stem Cell Rev Rep*. 2022;18(3):1025–1040. doi:10.1007/s12015-021-10176-0
24. Li X, Liu L, Yang J, et al. Exosome derived from human umbilical cord mesenchymal stem cell mediates MiR-181c attenuating burn-induced excessive inflammation. *EBioMedicine*. 2016;8:72–82. doi:10.1016/j.ebiom.2016.04.030
25. Zhang L, Ouyang P, He G, et al. Exosomes from microRNA-126 overexpressing mesenchymal stem cells promote angiogenesis by targeting the PIK3R2-mediated PI3K/Akt signalling pathway. *J Cell Mol Med*. 2021;25(4):2148–2162. doi:10.1111/jcmm.16192
26. He Y, Li Q, Feng F, et al. Extracellular vesicles produced by human-induced pluripotent stem cell-derived endothelial cells can prevent arterial stenosis in mice via autophagy regulation. *Front Cardiovasc Med*. 2022;9:922790. doi:10.3389/fcvm.2022.922790
27. Li Y, Zhang J, Shi J, et al. Exosomes derived from human adipose mesenchymal stem cells attenuate hypertrophic scar fibrosis by miR-192-5p/IL-17RA/Smad axis. *Stem Cell Res Ther*. 2021;12(1):221. doi:10.1186/s13287-021-02290-0

28. Wang D, Berg D, Ba H, et al. Deer antler stem cells are a novel type of cells that sustain full regeneration of a mammalian organ-deer antler. *Cell Death Dis.* 2019;10(6):443. doi:10.1038/s41419-019-1686-y
29. Li C, Suttie JM, Clark DE. Morphological observation of antler regeneration in red deer (*Cervus elaphus*). *J Morphol.* 2004;262(3):731–740. doi:10.1002/jmor.10273
30. Li C, Yang F, Sheppard A. Adult stem cells and mammalian epimorphic regeneration-insights from studying annual renewal of deer antlers. *Curr Stem Cell Res Ther.* 2009;4(3):237–251. doi:10.2174/157488809789057446
31. Min Yang L. Engineered antler stem cells derived exosomes potentiate anti-tumor efficacy of immune checkpoint inhibitor by reprogramming immunosuppressive tumor microenvironment. *Chem Eng J.* 2024;2024:1.
32. Guo Q, Liu Z, Zheng J, et al. Substances for regenerative wound healing during antler renewal stimulated scar-less restoration of rat cutaneous wounds. *Cell Tissue Res.* 2021;386(1):99–116. doi:10.1007/s00441-021-03505-9
33. Li C, Suttie JM, Clark DE. Histological examination of antler regeneration in red deer (*Cervus elaphus*). *The Anatomical Record. Disc Molecul Cell Evolut Biol.* 2005;282A(2):163–174. doi:10.1002/ara.20148
34. Rong X, Zhang G, Yang Y, et al. Transplanted antler stem cells stimulated regenerative healing of radiation-induced cutaneous wounds in rats. *Cell Transplant.* 2020;29:2138944253. doi:10.1177/0963689720951549
35. Rong X, Chu W, Zhang H, et al. Antler stem cell-conditioned medium stimulates regenerative wound healing in rats. *Stem Cell Res Ther.* 2019;10(1). doi:10.1186/s13287-019-1457-9
36. Li C, Clark DE, Lord EA, et al. Sampling technique to discriminate the different tissue layers of growing antler tips for gene discovery. *Anat Rec.* 2002;268(2):125–130. doi:10.1002/ar.10120
37. Yang M, Wang X, Pu F, et al. Engineered exosomes-based photothermal therapy with MRI/CT imaging guidance enhances anticancer efficacy through deep tumor nucleus penetration. *Pharmaceutics.* 2021;13(10):1593. doi:10.3390/pharmaceutics13101593
38. Franck CL, Senegaglia AC, Leite L, et al. Influence of adipose tissue-derived stem cells on the burn wound healing process. *Stem Cells Int.* 2019;2019:2340725. doi:10.1155/2019/2340725
39. Velnar T, Bailey T, Smrkolj V. The wound healing process: an overview of the cellular and molecular mechanisms. *J Int Med Res.* 2009;37(5):1528–1542. doi:10.1177/147323000903700531
40. Leavitt T, Hu MS, Marshall CD, et al. Scarless wound healing: finding the right cells and signals. *Cell Tissue Res.* 2016;365(3):483–493. doi:10.1007/s00441-016-2424-8
41. Baron JM, Glatz M, Proksch E. Optimal support of wound healing: new insights. *Dermatology.* 2020;236(6):593–600. doi:10.1159/000505291
42. Pakyari M, Farrokhi A, Maharlooie MK, et al. Critical role of transforming growth factor beta in different phases of wound healing. *Adv Wound Care.* 2013;2(5):215–224. doi:10.1089/wound.2012.0406
43. Wu D, Kang L, Tian J, et al. Exosomes derived from bone mesenchymal stem cells with the stimulation of Fe₃O₄ nanoparticles and static magnetic field enhance wound healing through upregulated miR-21-5p. *Int J Nanomed.* 2020;15:7979–7993. doi:10.2147/IJN.S275650
44. Kanji S, Das H. Advances of stem cell therapeutics in cutaneous wound healing and regeneration. *Mediators Inflamm.* 2017;2017:5217967. doi:10.1155/2017/5217967
45. Iso Y, Spees JL, Serrano C, et al. Multipotent human stromal cells improve cardiac function after myocardial infarction in mice without long-term engraftment. *Biochem Biophys Res Commun.* 2007;354(3):700–706. doi:10.1016/j.bbrc.2007.01.045
46. Burst VR, Gillis M, Putsch F, et al. Poor cell survival limits the beneficial impact of mesenchymal stem cell transplantation on acute kidney injury. *Nephron Exp Nephrol.* 2010;114(3):e107–e116. doi:10.1159/000262318
47. Di Bonzo LV, Ferrero I, Cravanzola C, et al. Human mesenchymal stem cells as a two-edged sword in hepatic regenerative medicine: engraftment and hepatocyte differentiation versus profibrogenic potential. *Gut.* 2008;57(2):223–231. doi:10.1136/gut.2006.111617
48. Lee RH, Seo MJ, Reger RL, et al. Multipotent stromal cells from human marrow home to and promote repair of pancreatic islets and renal glomeruli in diabetic NOD/scid mice. *Proc Natl Acad Sci USA.* 2006;103(46):17438–17443. doi:10.1073/pnas.0608249103
49. Inoue H, Murakami T, Ajiki T, et al. Bioimaging assessment and effect of skin wound healing using bone-marrow-derived mesenchymal stromal cells with the artificial dermis in diabetic rats. *J Biomed Opt.* 2008;13(6):64036–640310. doi:10.1117/1.3042266
50. Katsuda T, Kosaka N, Takeshita F, et al. The therapeutic potential of mesenchymal stem cell-derived extracellular vesicles. *Proteomics.* 2013;13(10–11):1637–1653. doi:10.1002/pmic.201200373
51. Wu L, Yuan W, Chen J, et al. Increased miR-214 expression suppresses cell migration and proliferation in Hirschsprung disease by interacting with PLAGL2. *Pediatr Res.* 2019;86(4):460–470. doi:10.1038/s41390-019-0324-9
52. Ren P, Wu NA, Fu S, et al. miR-122-5p restrains pancreatic cancer cell growth and causes apoptosis by negatively regulating ASCT2. *Anticancer Res.* 2023;43(10):4379–4388. doi:10.21873/anticancer.16634
53. Xie J, Wu W, Zheng L, et al. Roles of MicroRNA-21 in Skin Wound Healing: a Comprehensive Review. *Front Pharmacol.* 2022;13:828627. doi:10.3389/fphar.2022.828627
54. Siu MC, Voisey J, Zang T, et al. MicroRNAs involved in human skin burns, wound healing and scarring. *Wound Repair Regen.* 2023;31(4):439–453. doi:10.1111/wrr.13100
55. Chen L, Zhan CZ, Wang T, et al. Curcumin inhibits the proliferation, migration, invasion, and apoptosis of diffuse Large B-Cell lymphoma cell line by regulating MiR-21/VHL axis. *Yonsei Med J.* 2020;61(1):20–29. doi:10.3349/ymj.2020.61.1.20
56. Li J, Wei C, Yang Y, et al. Apoptotic bodies extracted from adipose mesenchymal stem cells carry microRNA-21-5p to induce M2 polarization of macrophages and augment skin wound healing by targeting KLF6. *Burns.* 2022;48(8):1893–1908. doi:10.1016/j.burns.2021.12.010
57. Xiao WR, Wu M, Bi XR. Ozone oil promotes wound healing via increasing miR-21-5p-mediated inhibition of RASA1. *Wound Repair Regen.* 2021;29(3):406–416. doi:10.1111/wrr.12907
58. Cheng S, Xi Z, Chen G, et al. Extracellular vesicle-carried microRNA-27b derived from mesenchymal stem cells accelerates cutaneous wound healing via E3 ubiquitin ligase ITC1. *J Cell Mol Med.* 2020;24(19):11254–11271. doi:10.1111/jcmm.15692
59. Liu J, Sun F, Wang X, et al. miR-27b promotes angiogenesis and skin repair in scalded rats through regulating VEGF-C expression. *Lasers Med Sci.* 2020;35(7):1577–1588. doi:10.1007/s10103-020-02991-7

International Journal of Nanomedicine

Dovepress

Publish your work in this journal

The International Journal of Nanomedicine is an international, peer-reviewed journal focusing on the application of nanotechnology in diagnostics, therapeutics, and drug delivery systems throughout the biomedical field. This journal is indexed on PubMed Central, MedLine, CAS, SciSearch[®], Current Contents[®]/Clinical Medicine, Journal Citation Reports/Science Edition, EMBase, Scopus and the Elsevier Bibliographic databases. The manuscript management system is completely online and includes a very quick and fair peer-review system, which is all easy to use. Visit <http://www.dovepress.com/testimonials.php> to read real quotes from published authors.

Submit your manuscript here: <https://www.dovepress.com/international-journal-of-nanomedicine-journal>